Volume 6, Issue 1, 2019, 119-127 **ISSN 2393-0586**

Biomaterials and Tissue Engineering Bulletin

http://btebulletin.com

https://doi.org/10.33263/BTEB61.119127

Original Research Article **Open Access Journal**

Received: 12.03.2019 / Revised: 29.03.2019 / Accepted: 2.04.2019/ Published on-line: 3.04.2019

Nano-mechanical properties of novel intermetallic coatings on 316L bioimplant material

Muhammad Ans[1,*], Muhammad Atif Makhdoom[2], Ali Hassan[2]

[1]Ecole Nationale Superieure des Mines de Saint-Etienne, France

[2] University of the Punjab Lahore, Pakistan

*corresponding author e-mail address: ***m_ans2002@yahoo.com***

ABSTRACT

In the present work, Nano-mechanical properties of intermetallic layer formed on 316L austenitic stainless steel have been investigated. Hot dip aluminizing technique applied on stainless steel samples for coating and composition of Al-Si alloys maintained as 8%, 10%, 12% and 14%. Nano-mechanical properties of the Intermetallic formed have been evaluated using Nano-indentation technique at room temp.era.tu.re and results were compared. On the basis of our observations and obtained results it is concluded that with increasing silicon percentage the thickness of the intermetallic layer increases. Howev.er, the Na.no-mechanical results showed that this layer is brittle in nature. Therefore, it can be inferred th.at for bio-implant application the thickness of the lay.er needs to be at lower level as possible.

Keywords: *hot-dip-aluminizing, intermetallic coating, biomedical applications, biocompatibility.*

1. INTRODUCTION

Hot-dip-aluminizing (HDA) is an impressive technique by which 316L stainless steel can be altered to heat resistant and oxidation. For sheets, the aluminizing takes place in a continuous process involving rolls and other equipment, whereas individual components are aluminized by dipping into molten aluminum for a specific length of time. The kinetics of the coating process are influenced by composition that used in aluminum melt, morphology and thickness as well as by that of the stainless steel being coated. The thickness and life of the coating in continuous and batch aluminizing are affected by the process parameters like temperature, time and handling (Awan et al., 2008).

Surface coating is an efficient and economical way to obtain desirable material properties by altering physical, chemical, or electrical characteristics of a material surface. The HDA, which is one of surface coating processes, is the most widely used method of coating a mild steel sheet with aluminum. The HDA is carried out to increase corrosion and oxidation resistance as well as hardness of the sheet. The method consists of dipping the sheet in a molten aluminum or aluminum alloy bath maintained at a fixed temperature for a certain period. The HDA is performed in industries mostly in a continuous way. For a continuous transport of the stainless-steel sheet during the HDA process, facilities such as a pot roll and a journal bearing are operated as being immersed in the molten metal bath (Kang et al., 2012).

Austenitic stainless steels are important class of the engineering material and widely used in many industries due its good properties like good corrosion and wear resistance. AISI-316L stainless steel have main content chromium and nickel and this is also called the chrome steel. This is a non-magnetic stainless steel and widely used in appliances and structural works. The austenitic stainless steel contains more than 12 percent of chromium. The amount of chromium present in stainless steel tells about its corrosion resistance. There are many fabrication processes used for AISI-316L stainless steel (Żaba et al., 2015).

The corrosion behavior in various artificial body fluids of various metals are examined by performing test in simulated body fluid, urine serum, blood plasma, simulated bile solutions, saliva prepared by artificially, Hank's, Cigada and Ringer' solution, Cigada evaluated with different type of metals such as nickel alloys, titanium alloys, zirconium metal, cobalt, chromium alloys, 316L stainless steel and Mg alloys etc. These are used for biomedical application and also as implant materials. The electrochemical corrosion tests carried out in selected body fluids (Bansiddhi et al., 2008). For bone implantation and surgery these metals/ alloys have been used. The artificial body fluids are always found in human body in form of blood plasma and saliva and made from different compositions that is important aspect to be noted while choosing implant material because, implant materials may be directly affected by these body fluids and start depleting of ions could be toxic for human body (Mary and Rajendran, 2012).

Biodegradable magnesium alloys–a new class of degradable biomaterials – may be promising candidates and have recently attracted much attention. In contrast to commonly used titanium or steel implants, biodegradable magnesium alloys obviate the need for a second surgical intervention for implant removal and minimize stress shielding effects due to their elastic modulus, which is close to that of bone. Furthermore, biodegradable 316L stainless steel is more suitable for load-bearing applications due to their excellent mechanical and corrosion resistance properties (Castellani et al., 2011).

2. MATERIALS AND METHODS

2.1. Material selection

316L Stainless steel sheet of 2 mm thickness and 25×50 mm dimensions purchased from the market.

2.2. Preparation of aluminum alloy melts

Some of the initial experiments were conducted in an electrically heated pit-type furnace. However, it was observed that during the aluminizing of 50mm long specimens, it was difficult to maintain the temperature over the entire length of the specimens. Hence, a gas-fired furnace with a double burner was used.

The aluminum silicon alloy was melted in a graphite crucible in a gas fired-furnace in which the temperature could be controlled to within ±5°C with the help of a K-type thermocouple. The molten aluminum alloy was blanketed with a layer of KCl-NaCl-Na_2F flux. The constituents adjusted in such a way that suitable melting temperature can be achieved. The dipping was carried out at temperature 850°C. Before every coating experiment, the temperature was carefully measured and controlled at the required level. After giving required time the samples taken out and hung to drop the temperature. Aluminizing was carried out in aluminum silicon alloy melt prepared by melting electrical grade conductor of aluminum that was available in small cut-pieces. The additions of silicon were made by adding calculated quantities of Al-50% Si master alloy. The actual composition of the melt was also obtained by taking small samples from the molten alloy which was later analyzed on a 'METOREX' ArcMet930 Spark Emission Spectrometer.

2.3. Cleaning/fluxing prior to aluminizing

The samples were cleaned by the process of sonication. In this method sample dipped in Ethanol and IPA (propane-2) for 10/10 minutes each. Then they mechanically cleaned sample were carefully treated/pickled in a 50% diluted solution of HCl, rinsed in running water and then in methanol, then immediately dipped in aluminized bath. The method provided an easy and yet very effective method of cleaning for the present purpose. However, it must be realized that whereas this method can be safely used for carefully handled individual research specimens, the method was clearly not easy to follow in a commercial aluminizing process.

2.4. Coating

The 316L stainless steel sheet cut into small pieces with dimensions 25mm X 50mm. a small hole drilled at the center of each strip and hanged with wire. All the samples were cleaned by following process: first dipped in nitric acid to remove any oil or grease and then washed with tap water followed by cleaning in ethanol. Four melts of Al-Si alloy with varying percentages of 8%, 10%, 12% and 14% silicon were prepared in pit furnace. Clean samples of stainless steel 316L was immersed in the melts for 2 minutes at 750°C. Samples divided in two groups, one for diffusion by siliconizing and other group subjected to different characterization technique for evaluation of intermetallic.

2.5. Characterization techniques

2.5.1. Metallographic

All the samples were sectioned by diamond disc cutter and cold mounted vertically followed by sample preparation. The specimens were grinded on 80, 120, 180, 320 400, 600, 800, 1000 and 1200 grit size paper for rough grinding. Final polishing was done using 3µ and 6µ diamond pastes on Teflon cloths. After polishing there is no need of etching the samples as we can directly get microstructures on optical microscope.

Microscopic examination of the polished and etched samples was carried out on an Olympus GX-one camera microscope. This microscope was fitted with a 'Motiram' digital camera coupled with a computer. The various magnifications were calibrated with the help of a stage micrometer.

Specimens subjected to studied metallographically to examine the behavior of interlayer. For this purpose, the samples sectioned across the line of the cracking observed on the specimen surface. Different series of emery papers were used, and then polished surface were examined at different angles to check the inter layer.

2.5.2. Nano-indentation

The continuous stiffness measurement (CSM) is an established method for evaluating elastic modulus and hardness continuously during indentation. Nano-indentation process applied to measure the hardness of coating. After HDA the hardness of coating of all samples with different compositions investigated on nano-indentor hardness machine. When evaluating mechanical properties of a coated specimen then the main concern is the relations between mechanical properties of coating and substrate. Generally, lower the coating thickness, higher will be the involvement of substrate. Therefore, micro-hardness experiments on thin coatings are carried out with very small loads. At lower loads the high measured hardness is due to the formation of Geometry density dislocations (GND). However, indentation depth if is tiny as compared to tip size then surface properties of material are of particular interest.

2.5.3. SEM and EDX micrographs

In order to find the variation in the chemical composition with the coating thickness and inside the steel, EDX is carried out with close spacing. It is interesting to note that the variation in the chemical composition is m ore in case of diffused samples and migration of Iron and chromium is more outward in coating as compared to inward diffusion of aluminum and steel. However, a step by step move to equilibrium composition close to coating/substrate interface corresponds to decrease in coating growth rate. Nevertheless, of the fact that an increase in the silicon percent in the coating enhances the coating thickness but the diffusion of the aluminum inside the lattice is hindered by Si. Silicon acts as a diffusion limiting agent for Fe and Cr. Reason for this is the high electron affinity of Si towards Fe. Similar results were evident in other studies (Yun et al., 2017). Intermetallic formed due to variation in thickness and composition. Detail of all coatings is the part of future publication. Only one result is explained here. All the points where the EDX were taken is shown in SEM micrograph (Fig 11 in the section 3.2.1) with the results of intermetallic formed at specified locations. The detail study of the Nano-mechanical properties and correlation of the same with microstructure is explained in subsequent sections

2.5.4. Diffusion of coated samples/siliconizing

Diffusion technique applied on coated samples. This is recent technique of heat treatment of samples but inside the silica sand. Round balls of silica sand and clay were made coated samples after HDA positioned in these balls and then placed into muffle furnace at 500 C for 1 hour. This technique is known as siliconizing at the temperature silica allow the intermetallic coating to make strong bond around the steel substrate and thickness of intermetallic also affected. Hardness test performed after this activity results gained were conferring to our prerequisite.

3. RESULTS AND DISCUSSIONS

3.1. Microstructural characterization of coated samples

Figure 1 shows that three regions such as coating, intermetallic and steel substrate. In this structure aluminum migrates toward the substrate and iron element migrate outer side of the surface. When aluminum and iron to meet made the intermetallic layers but the percentage of silicon in this aluminum melts 8% therefore, we can demonstrate that their intermetallic layer thickness more as compared to others the aluminum alloy melts (Awan and Hasan, 2008). The structure shows that their crystal of silicon which were not completely dissolved in intermetallic layer. The intermetallic layer always made toward the substrate. Mostly alloy layer thickness range as compared to the intermetallic layer more. In this coating process the time was 120 seconds.

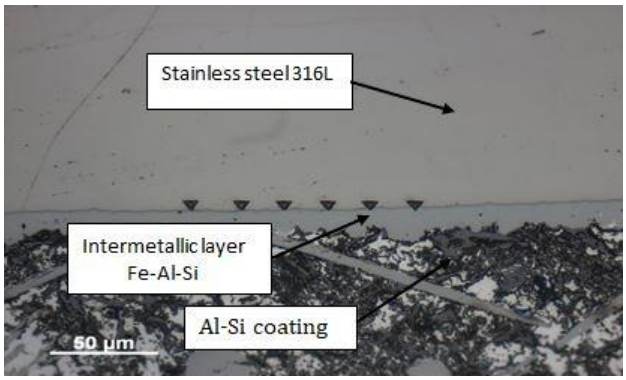

Figure 1. Microstructure of 8% Al-Si Alloy coating

Figure 2 shows that the same regions in this metallography structure in 10% Al-Si alloy here difference in thickness clearly show that as the percentage of Si increases the thickness also effected and intermetallic layer also increases. The time given to this activity was also same as given to other samples.

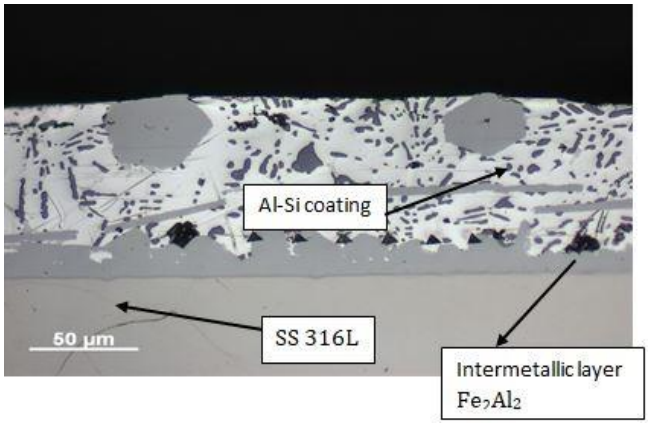

Figure 2. Micrograph of 10% Al-Si alloy coating

It seems clearly in Figure 3 as the percentage of silicon increases the thickness also increases. Here the percentage of carbon in substrate also affected the intermetallic layer and alloy structure due to pearlite dispersion. The pearlite then converted into martensitic due to difference in liquid melt. The intermetallic range at 12% aluminum silicon alloys.

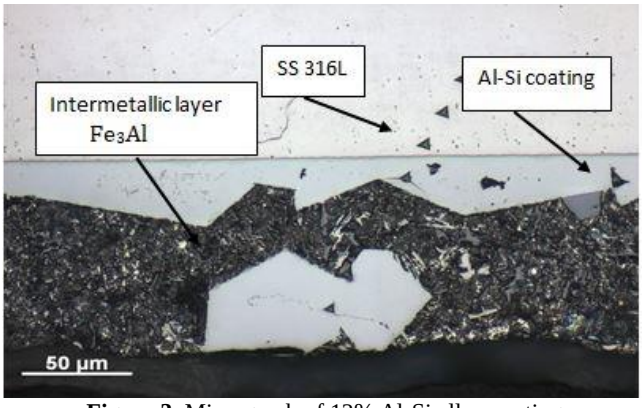

Figure 3. Micrograph of 12% Al-Si alloy coating

Figure 4 present very important relation as compared to other aluminum silicon alloy structure. The condition was different as compared to other aluminum silicon alloys and the thickness of intermetallic layer was much increased. The reason is the variation of Si in alloy and time. Time relation and silicon percentage directly proportional to the intermetallic layer thickness. Because of the time increased so that the aluminum iron and silicon made strong intermetallic bond. The time given to this activity was 3 minutes and percentage of Si was 14%.

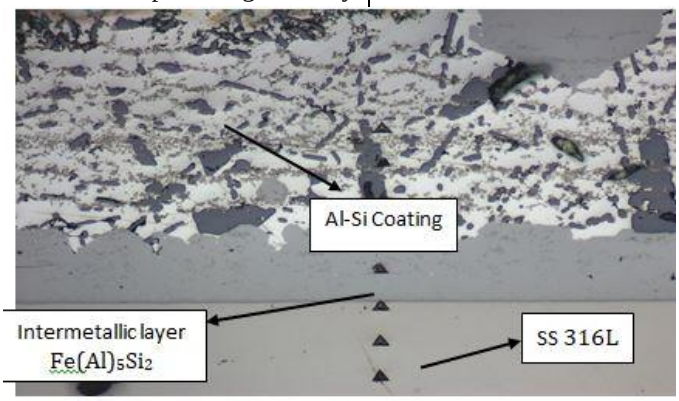

Figure 4. Micrograph of 14% Al-Si alloy coating

3.2. Diffused and non-diffused samples

316L stainless steel in molten Al-Si alloys developed coating as shown in microstructures obtained using optical microscopy (Figure 5-10). Cross sectioning examination shows three different zones namely, steel substrate, coating and the remnant of Al-Si alloy adhered to the coating after dipping. It is clear from the figure that coating thickness increases as the percentage of the silicon increases. It is further evident from the reduction in the thickness of coating after diffusion process that aluminum and silicon atoms has find the way to diffused into the iron lattice of stainless steel (Othman et al., 2015). Variation in the thickness of coatings is shown in Table 1.

Table 1. Comparison of diffused and non-diffused coated samples

Al-Si Alloy	10%	12%	14%
Non-Diffused	105.11µm	217.52µm	270.78µm
Diffused	86.51µm	98.87µm	203.82µm

Figure 5. Microstructure of non-diffused sample 10% Al-Si

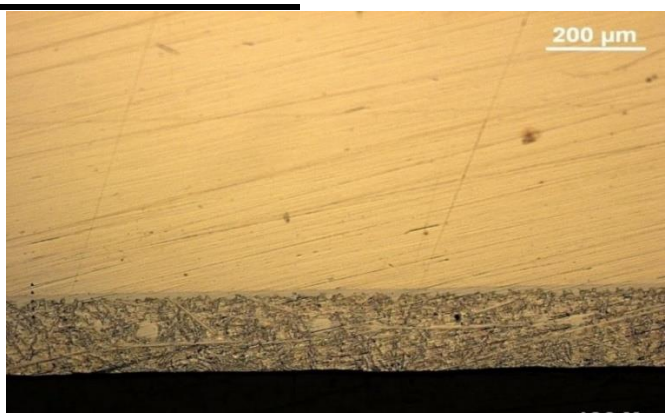

Figure 6. Microstructure of diffused sample 10% Al-Si

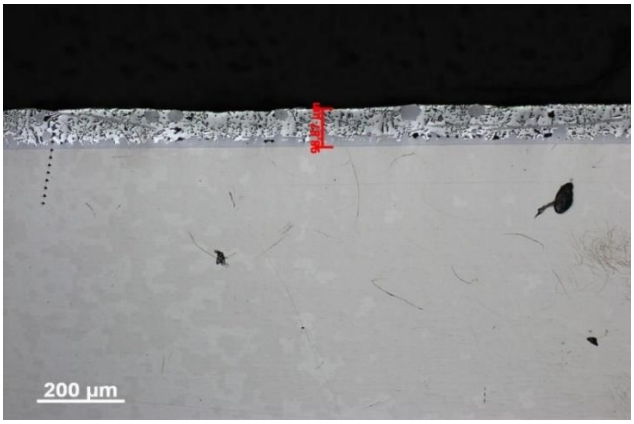

Figure 7. Microstructure of diffused sample 12% Al-Si

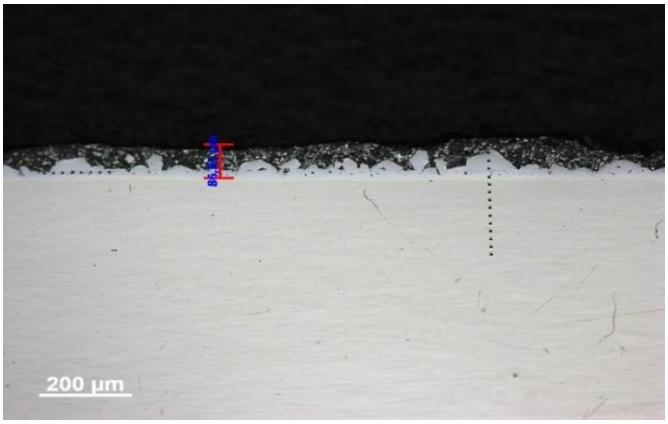

Figure 8. Microstructure of non-diffused sample 12% Al-Si

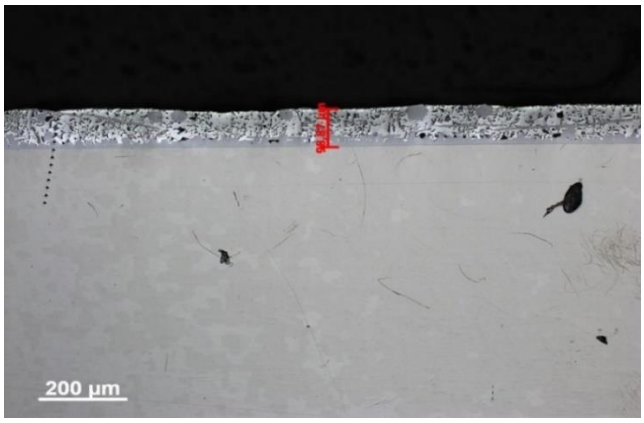

Figure 9. Microstructure of diffused sample 14% Al-Si

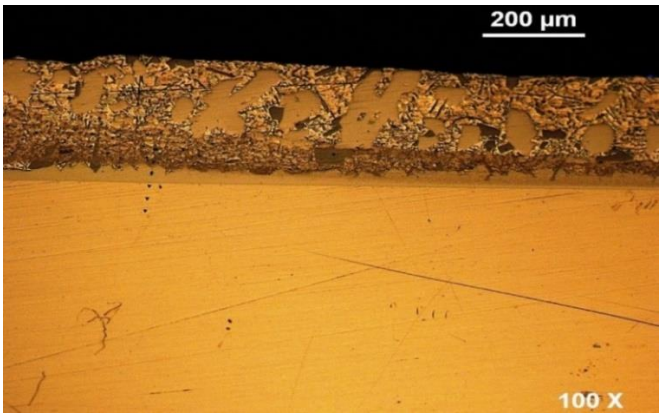

Figure 10. Microstructure of non-diffused sample 14% Al-Si

Figure 11 shows a close view of the indentation at nanoscale. A crack can be observed at the intermetallic layer adhere to the metal. The interesting thing to note that this crack runs along the parallel direction with in this phase only and did not penetrated the metal and not even the Al-Si coating. The same behavior is observed for all other Si percentage samples.

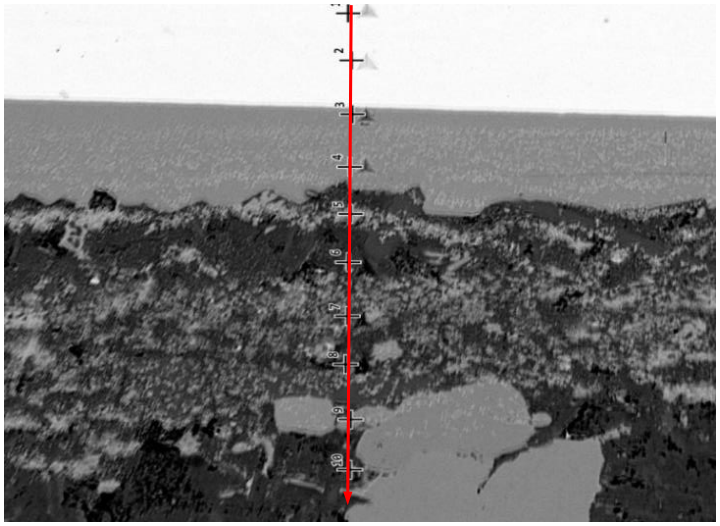

Figure 11. SEM micrograph of non-diffused sample 14% Al-Si (Spot 3 = $Fe(Al)_3Si$; Spot 4 = $Fe(Al)_5Si_2$; Spot 5 = Al_4Si_3Cr; Spot 6 = Al_7Si_2Ni; Spot 7 = Al_3Si; Spot 8 = Al_3Si; Spot 9 = $Al_{13}Si_9Fe_2Cr$; Spot 10 = Al)

3.3. Properties Evaluation vs Nano-Indentation

The continuous stiffness measurement (CSM) is an established method for evaluating elastic modulus and hardness continuously during indentation. This is based on the hypothesis that the imposed oscillatory excitation of the indenter did not affect the properties of material under inspection. When evaluating mechanical properties of a coated specimen then the main concern is the relations between mechanical properties of coating and substrate.

Figure 12 shows a close view of the indentation at nanoscale. A crack can be observed at the intermetallic layer adhere to the metal. It is interesting to note that this crack runs along the parallel direction with in this phase only and did not penetrated into the metal and not even the Al-Si coating. The same behavior is observed for all other Si percentage samples.

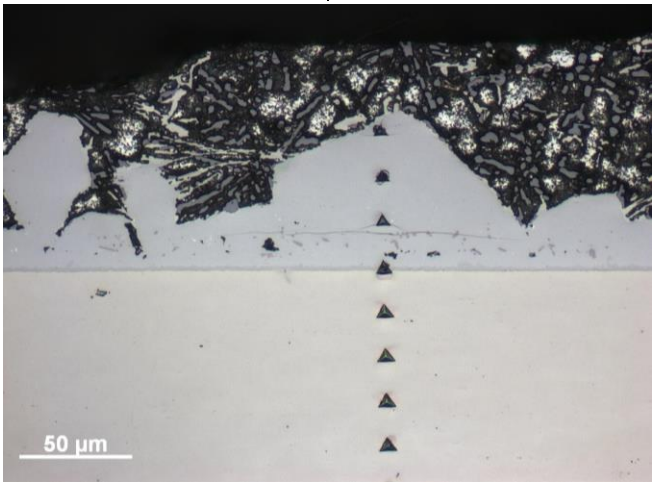

Figure 12. Nano-indentation close view of diffused sample 12% Al-Si

The graph illustrated in Figure 13 shows the trend in hardness as move from case to core (metal). Hardness of coating increases to a maximum value and then decreases and attain a constant trend. The initial value at the start is of pure Al-Si alloy at the outer periphery but the higher hardness is recorded for the intermetallic and these are considerably higher than the base metal itself. The higher hardness value is assumed to be responsible for the brittleness of the coating as the crack has appeared in the reign only. To evaluate this effect in more detail a comparison is made between the diffused and non-diffused samples. Comparison showed that the non-diffused sample has developed a relatively soft intermetallic and crack has not been developed while indentation. A comparison of diffused and non-diffused samples of Al-Si 14% is shown in Figure 14 and 15.

A similar trend is observed in all other coatings as shown in the graphs illustrated in Figure 16 and 17.

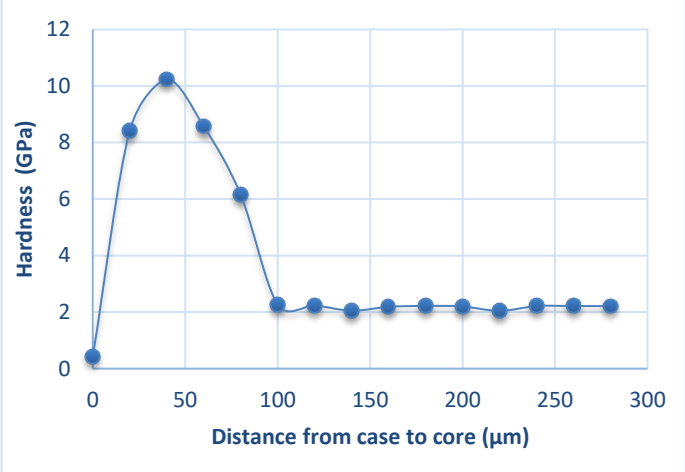

Figure 13. Hardness profile of diffused sample 12% Al-Si

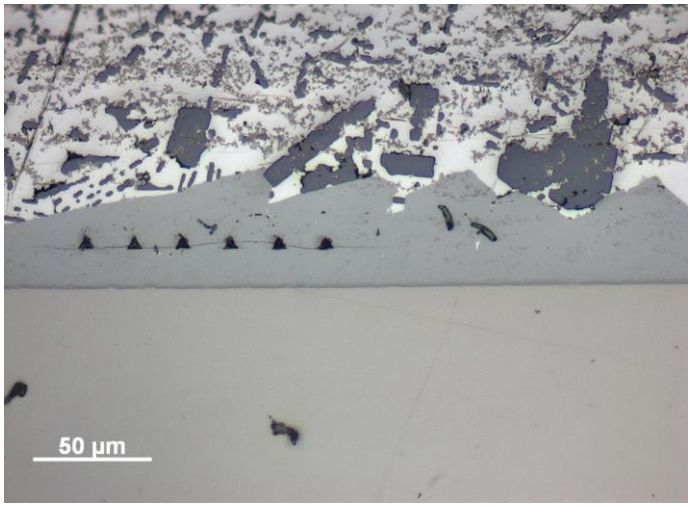

Figure 14. Nano indentation close view of diffused sample 10% Al-Si

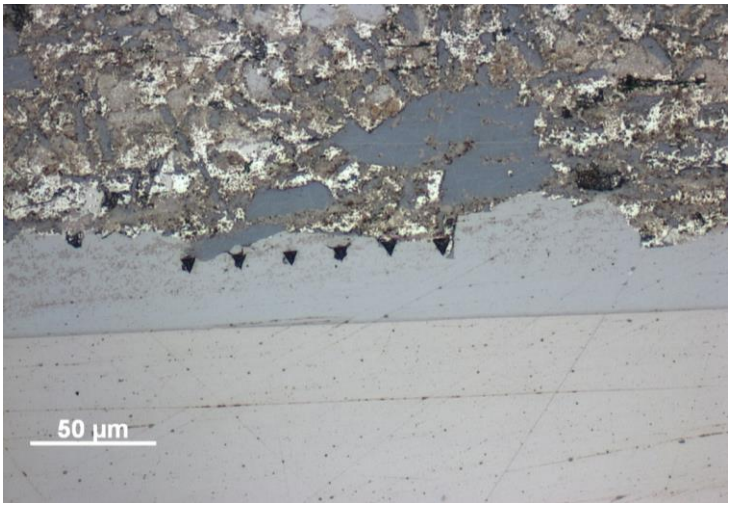

Figure 15. Nano indentation close view of non-diffused sample 14% Al-Si

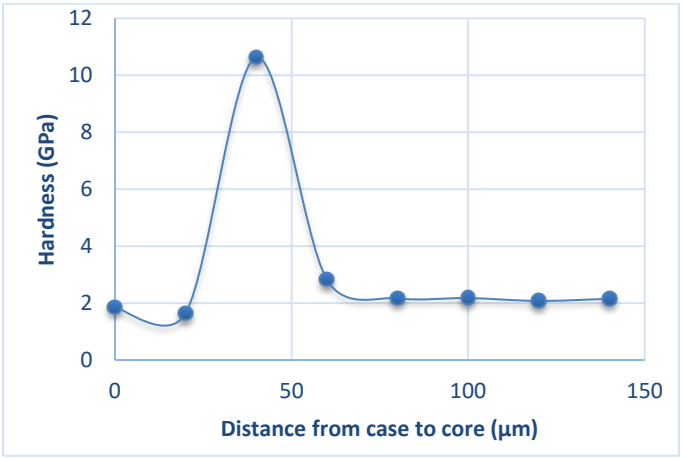

Figure 16. Hardness profile of diffused sample 10% Al-Si

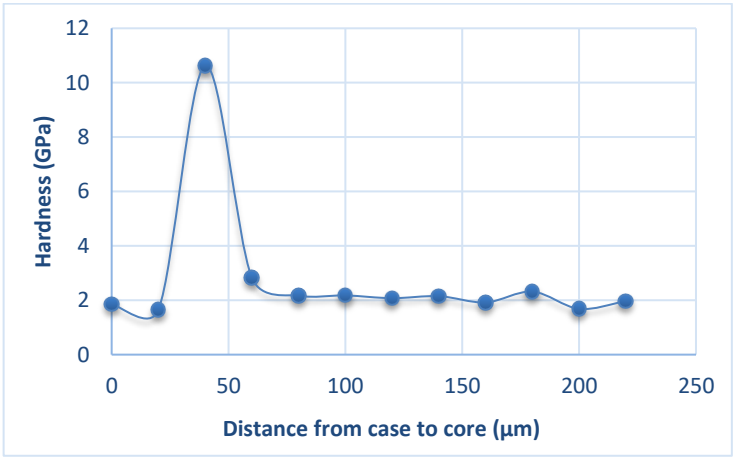

Figure 17. Hardness profile of diffused sample 14% Al-Si

Figure 18 shows the variation in elastic and shear modulus as move from case to core. It can be noted that the both the modulus has variation in their values in the coating regions. This is again due t the variable in composition in the coatings due to inward and outward diffusion of the alloying elements. A constant value is observed in base metal after a measured depth of 150 µm. It is interesting to note that the modulus of the coating is comparable to the base metal and somehow it is relatively lower than that of the base metal which is about 222 GPa. Nevertheless, the fact that the modulus of coating is much higher than that of bone (which is about 10-20 GPa) but it is very useful for the mechanical response to it. This is because that the resulting gradient of modulus at bone/metal interface helps in transferring the load and hence reducing the so-called "stress shielding effect". The said effect is a clinical complication considered for extreme desorption of implanted bone and arises due to the difference in the elastic modulus of implant and natural bone (Rubash et al., 1998).

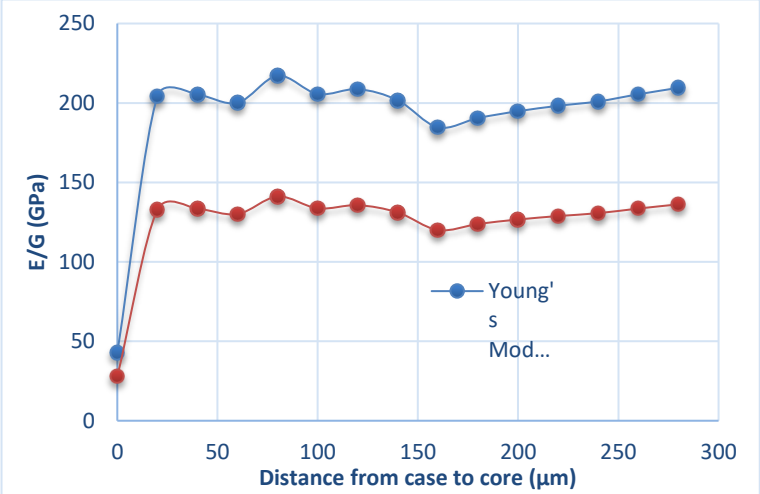

Figure 18. Elastic and shear modulus profile of diffused samples

3.4 Properties evaluation vs corrosion

Corrosion analysis of the samples was carried out under simulated body fluid i.e Ringer's solution at body temperature (37 C). Electrochemical impedance spectroscopy (EIS) along with Potentiodynamic polarization technique has been utilized to evaluate the electrochemical corrosion behavior of both coated and uncoated samples. EIS results are analyzed using Equivocate fitting program.

Figure 19 shows the behavior of coated and non-coated sample after 15 minutes immersion in the Ringer solution. Potentiodynamic polarization curves of both the samples depict passivity in anodic region. This may be attribute to passive behavir under test conditions of intermetallic steel compound i.e. $Al_{12}(Fe, Cr)_3Si_2$ that has formed at the interface of the steel and coating. Under passive behavior it is difficult to evaluate the corrosion response of the material and therefore it is determined by current density. Nevertheless, the fact that both coated and non-coated samples show the similar values i.e. 1.039 X 10^{-7} A/cm2 but propensity to localized attack can also be evaluated by the length of passive branch. On the basis of this technique it is revealed that non-coated sample demonstrates nobler behavior than that of coated one. i.e -216 and -425 mV/SCE respectively. The pitting potential (E_{pit}) for the coated sample is about -155 mV/SCE which is much lower than the uncoated sample whose value is 693 mV/SCE. Therefore, the length of passivity for coated specimen is shorter than the non-coated one i.e. 580 vs 909 mV respectively. It is therefore deduced that the coated samples demonstrate higher susceptibility to localized corrosion after short immersion i.e 15 min than that of non-coated sample. However, they both have same passivation current density and similar corrosion rate.

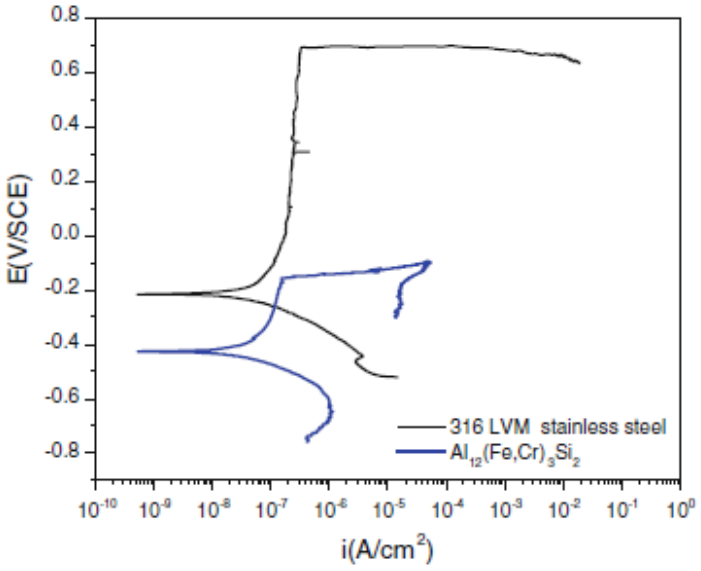

Figure 19. Polarization curves of coated and uncoated stainless steel

On the other hand, after one week both the curves i.e coated, and non-coated samples depict active and followed by passivation behavior as shown in Figure 20. The curve shows an increase in corrosion potential up to 600 mV and then a steady state reached in both the samples and continues until pitting potential is reached. This shape of the curve demonstrates the growth of an oxide layer while in active phase. This grown oxide layer is attributed to the passive behavior under oxidizing environment. It is further noted that the corrosion potential of coated sample shifts towards more cathodic values with time i.e. -754 mV/SCE but E_{corr} of non-coated sample increases to more nobler values with time i.e. -152 mV/SCE as compared to its previous initial E_{corr} value. I_{corr} values of both materials were estimated from Tafel slopes i.e 7.49 X 10^{-9} and 3.29 X 10^{-9} A/cm^2 for coated and uncoated samples respectively which are lower than initial I_{corr} values for both samples by two order of magnitude. This demonstrates that as the time passes, the protective oxide layer get coarsened and thereby reduces the electrochemical activity. Also, shift of pitting potential (about 1V) towards nobler values for the coated sample after 1 week is comparable to the bare steel i.e. 876 mV/SE. This behavior depicts a remarkable improvement in propensity of localized corrosion (Gurappa, 2002).

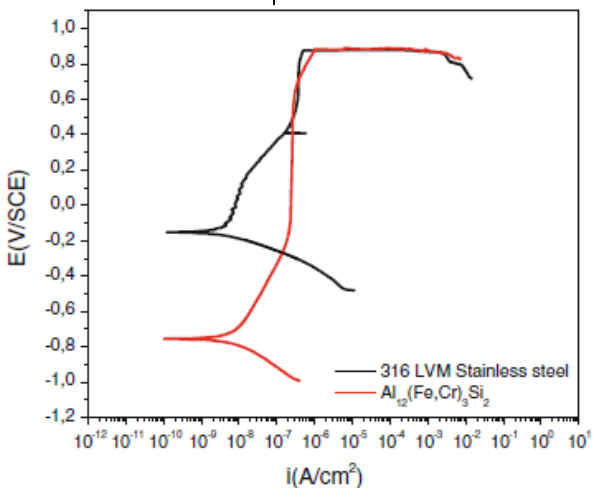

Figure 20. Polarization curves of coated and uncoated stainless steel (after one week)

Impedance spectroscopy has also been utilized for the stability evaluation of coating in Ringer's solution. The spectrum obtained by this technique is shown in Figure 21 and 22. It can be seen that the uncoated sample depicts one constant time for all immersion time at bode phase angle plot and a phase angle of -85 is for almost all the frequency range. The capacitance value of about 8.6l F/cm^2 has been calculated using equations found in the literature (Walter, 1986). On the other hand, the Bode phase diagram for the coated sample reveals two different time constants at the initial stage. One maximum time constant demonstrated at medium–high frequencies approximately at -85 with 1.5l F/cm^2 capacitance value while another appears at low frequencies. With increasing immersion time, contribution of low frequency vanishes while maxim um placed at medium–high frequencies become broadened. The capacitance value of about 5.5l F/cm^2 for both the samples, due to the evolution of impedance at the initial stage of the test demonstrates metal/oxide double layers presence as it is typical for the presence of such bi-layers. At the same time, a difference is also noted in the modulus of impedance Bode diagrams for both types of samples.

Non-coated sample demonstrate a slope of -0.94 at medium–low frequencies (Walter, 1986). On the other hand, two different slopes at different linear stages are observed for coated sample and it is due to the two distinct contributions observed in the phase angle plots. A slope value of -0.92 has been observed at medium–high frequencies but a significant decrease is observed from 1 Hz suggesting the presence of a diffusion response. The development of /Z/ Bode plot with respect to time demonstrates that the vanishing of low frequency response leads to a nearly pure capacitive behavior and this can be simulated using an equivalent circuit consisting a resistor that is connected with a capacitor in series. But the experimental results deviate from the ideal values that can be obtained by such an equivalent circuit.

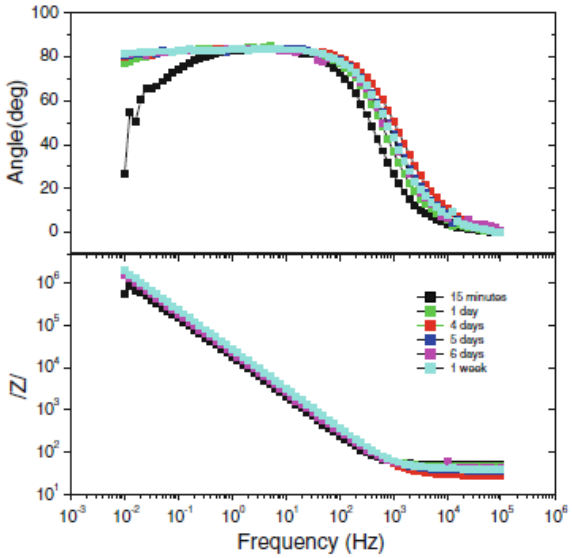

Figure 21. Impedance spectra corresponding to uncoated samples

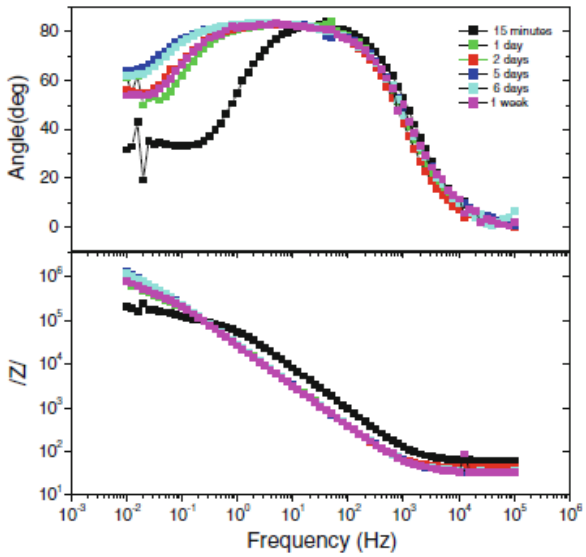

Figure 22. Impedance spectra corresponding to coated samples

4. CONCLUSIONS

In HDA the intermetallic layer gained consists of mainly Fe_2Al_5 phase between. The growth of inter-layers into the steel substrate found as finger-like columnar crystals, oriented perpendicular to the surface being aluminized. These orientations in the form of columnar finger-like crystals exhibit a preferred lattice such that is normal to the substrate surface and along the longitudinal axis of the columnar crystals.

Diffusion treatment makes the coating brittle and it is thought to be due to the formation of complex intermetallic.

High hardness and modulus are observed in the intermetallic zone containing Fe-Al-Si in varying composition as intermetallic.

Aluminum has reactive properties naturally; by addition of silicon we can decrease its reactivity. On increasing Si content specimen become less active and rate of corrosion decreases.

It is observed that intermetallic compounds registered the same corrosion rate as that of stainless steel in Ringer's solution. However, resistance to localized attack is more.

5. REFERENCES

Awan, G. H., Ahmed, F., Ali, L., Shuja, M. S. & Hasan, F. 2008. Effect of coating-thickness on the formability of hot dip aluminized steel. *Pak. J. Engg. & Appl. Sci*, 2.

Awan, G. H. & Hasan, F. U. 2008. The morphology of coating/substrate interface in hot-dip-aluminized steels. *Materials Science and Engineering: A,* 472**,** 157-165.

Bansiddhi, A., Sargeant, T. D., Stupp, S. I. & Dunand, D. C. 2008. Porous niti for bone implants: A review. *Acta Biomater,* 4**,** 773-82.

Castellani, C., Lindtner, R. A., Hausbrandt, P., Tschegg, E., Stanzl-Tschegg, S. E., Zanoni, G., Beck, S. & Weinberg, A. M. 2011. Bone-implant interface strength and osseointegration: Biodegradable magnesium alloy versus standard titanium control. *Acta Biomater,* 7**,** 432-40.

Gurappa, I. 2002. Characterization of different materials for corrosion resistance under simulated body fluid conditions. *Materials Characterization,* 49**,** 73-79.

Kang, S., Han, K., Kim, K., Kang, Y., Son, K. & Kim, D. 2012. *Formation behavior of an intermetallic compound layer during the hot dip aluminizing of cast iron*.

Mary, J. S. & Rajendran, S. 2012. Corrosion behavior of metals in artificial body fluid an over view. *Zaštita materijala,* 53**,** 181-189.

Othman, M., Yusnenti, F. & Mohdyusri, I. 2015. Siliconizing process of mild steel substrate by using tronoh silica sand (tss): An experimental investigation. *Procedia CIRP,* 26**,** 554-559.

Rubash, H. E., Sinha, R. K., Shanbhag, A. S. & Kim, S. Y. 1998. Pathogenesis of bone loss after total hip arthroplasty. *Orthopedic Clinics of North America,* 29**,** 173-186.

Walter, G. 1986. A review of impedance plot methods used for corrosion performance analysis of painted metals. *Corrosion Science,* 26**,** 681-703.

Yun, J.-G., Lee, J.-H., Kwak, S.-Y. & Kang, C.-Y. 2017. Study on the formation of reaction phase to si addition in boron steel hot-dipped in al–7ni alloy. *Coatings,* 7**,** 186.

Żaba, K., Nowosielski, M., Kita, P., Kwiatkowski, M., Tokarski, T. & Puchlerska, S. 2015. Effect of heat treatment on the corrosion resistance of aluminized steel strips. 60**,** 1825.

6. ACKNOWLEDGEMENTS

The authors wish to express their thanks for the financial support of grants to University of the Punjab, Lahore and Ecole des Mines, France.

7. CONFLICTS OF INTEREST

The authors declare no conflict of interest.